Macromolecules

pubs.acs.org/Macromolecules Article

Chain Conformations of TEMPO-Based Organic Radical Polymers with Varying Radical Loading and Temperature in Battery-Relevant Solvents

Md Ashraful Haque, Alexandra D. Easley, Josh G. Moncada, Jodie L. Lutkenhaus, and Mark D. Dadmun*

Cite This: Macromolecules 2024, 57, 6333−6343 Read Online

ACCESS | Metrics & More | Article Recommendations | Supporting Information

ABSTRACT: Poly(2,2,6,6-tetramethylpiperidinyloxy-4-yl methacrylate) (PTMA) is an organic radical polymer that is a promising active material in organic batteries. The proximity of the radical groups impacts the nature of charge transfer, in which closer packing promotes electron exchange; however, the chain conformation of PTMA is not well understood. Here, the conformation of PTMA in, and its thermodynamic interactions with, battery-relevant solvents is determined using small-angle neutron scattering (SANS). *N*-methyl-2-pyrrolidone (NMP) and 50:50 (wt %) ethylene carbonate/dimethyl carbonate (EC/DMC) mixtures with PTMA of varying radical content (68 vs 98%) and temperature (25 and 60 °C) are examined. Both solvents are theta solvents for PTMA irrespective of radical loading and temperature. PTMA attains an expanded chain conformation in NMP and a more compact polymer chain conformation in EC/DMC. Finally, the electrochemical performance of PTMA films formed from EC/DMC shows improved performance relative to those cast from NMP, which is interpreted to indicate that the compact conformation of PTMA in EC/DMC enables improved inter- and intrachain charge transfer.

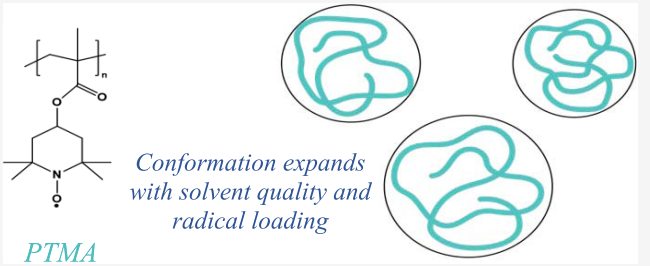

INTRODUCTION

Recently, the demand for polymer-based energy storage systems (ESSs) has been rapidly increasing as a sustainable replacement for the frequently used Li-ion batteries.[1,2] In current Li-ion batteries, the cathode usually consists of inorganic transition metal oxides such as manganese, nickel, and cobalt, which are found in a finite quantity in nature. Moreover, Li-ion battery materials suffer from supply chain issues, poor recyclability, and toxicity.[3−5] Hence, it has become imperative to look for potential replacements of these traditional materials used in Li-ion batteries. Active materials based on organic redox-active moieties can serve as a potential replacement in Li-ion batteries due to their demonstrated performance in organic solid state and flow batteries.[6−8]

Organic radical polymers often consist of a redox-active pendant group with a stable free radical that controls the charge transport and a polymer backbone, which in turn controls the thermal and mechanical properties of the polymer.[9] The redox-active pendant group of the organic radical polymer can undergo reversible redox reactions allowing them to serve as alternative materials to the inorganic materials used in Li-ion batteries.[6] Among a myriad of organic radical polymers, poly(2,2,6,6-tetramethylpiperidinyloxy-4-yl methacrylate) (PTMA) is commonly studied for its ease of synthesis, fast charge transport kinetics, and high theoretical capacity of 111 mAh g^{-1}.[10] Unique structural features of the PTMA redox-active moiety, 2,2,6,6-tetramethyl-1-piperidinyloxy (TEMPO), include its stable nitroxide radical state that, during the charging process, can convert to either oxoammonium cation or to the aminoxyl anion when utilized as a cathode or anode, respectively. The reversible redox reaction of PTMA has been capitalized to observe an operational capacity of almost 100% of its theoretical capacity.[11]

PTMA has been used as a redox-active material for organic batteries and ESSs; however, there is a lack of knowledge related to the conformation of this nonconjugated material and charge transfer mechanisms. With this in mind, the conformation of PTMA during the fabrication and operation of batteries is of interest to further understand the factors impacting charge transfer in organic radical polymers. Previously, small-angle neutron scattering (SANS) has been used to reveal the structure of various amorphous polymers in solution and the melt.[12−14] Using SANS, our previous study examined the conformation of PTMA in acetonitrile, documenting the change in PTMA conformation and assembly as a function of radical loading and the oxidation level.[15] However, the conformational changes can also impact the

Received: May 19, 2024
Accepted: June 12, 2024
Published: June 25, 2024

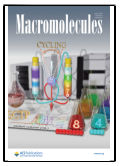

https://doi.org/10.1021/acs.macromol.4c01134
Macromolecules 2024, 57, 6333−6343

Table 1. Summary of the Synthetic Conditions, Degree of Polymerization, Molar Mass, Dispersity, and Radical Loading for the Synthesized PTMA Samples

polymer name	TMPM/CTA/AIBN[a]	oxidation method	DP[c]	M_n (kDa)[c]	$Đ$[c]	radical loading (%)[d]
PTMA-15−72	13:1:0.3	H_2O_2	15	3.5	1.2	72
PTMA-44−87	33:1:0.3		44	10.6	1.2	87
PTMA-122−95	98:1:0.3		122	29.2	1.2	95
PTMA-277−98[b]	330:1:0.7		277	66.6	1.7	98
PTMA-276−68[b]	330:1:0.7	mCPBA	276	66.2	2.1	68

[a]Molar ratio. [b]Synthesized using 2-phenyl-2-propyl benzodithioate as a CTA. [c]Determined using SEC in THF against a polystyrene standard. [d]Determined using EPR spectroscopy.

Scheme 1. Synthetic Route for PTMA-X-R Samples Using 4-Cyano-4 (((dodecylthio)carbonothioyl)thio)pentanoic Acid as the CTA

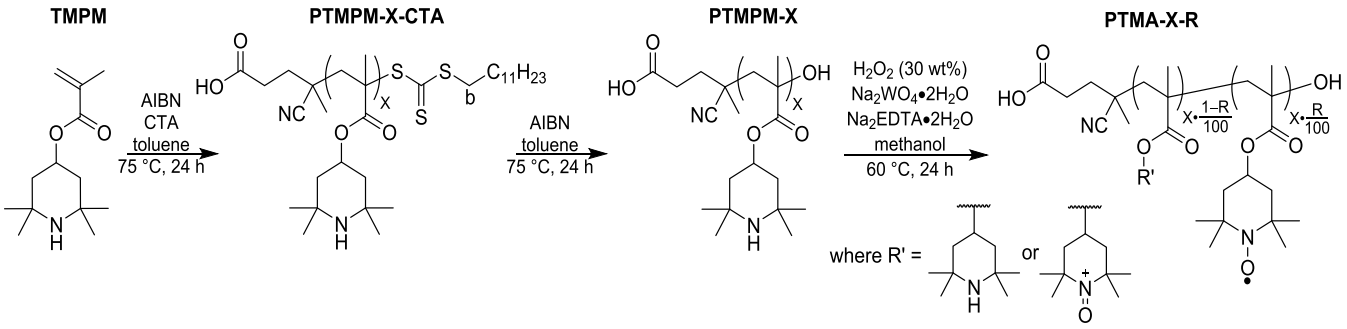

performance of PTMA-based electrodes. Therefore, we seek to expand these studies to provide more direct information on the conformation and structure of PTMA in battery-relevant solvents. For example, the performance of a PTMA cathode in a commonly used battery solvent such as carbonates fades after a certain number of cycles resulting in poor battery efficiency.[16] Moreover, in order to construct the PTMA cathode for an organic radical battery, the PTMA must be dissolved in a suitable solvent. *N*-methyl-2-pyrrolidone (NMP) is commonly used to process PTMA as an electrode due to its thermal stability and low volatility.[17−19] Frequent use of NMP as a solvent to fabricate PTMA-based cathodes further motivates the examination of PTMA conformation in NMP to provide molecular-level insight into the correlation of its performance in a battery to molecular conformation.

Here, we use SANS to elucidate the conformation and thermodynamic interactions of PTMA in NMP and a 50:50 mixture of ethylene carbonate and dimethyl carbonate (EC/DMC). We utilized deuterated solvents to improve the contrast between polymer and solvent, thus enabling the investigation of the conformation of PTMA in dilute solution using SANS. In this current study, the radical loading of PTMA is varied by using different oxidizing agents (meta-chloroperoxybenzoic acid and H_2O_2). The conformation and polymer−solvent interactions of PTMA in deuterated NMP and a 50:50 mixture of deuterated ethylene carbonate and deuterated dimethyl carbonate (EC/DMC) at room temperature (RT) and at 60 °C were investigated. Analysis of the scattering data by a Zimm plot analysis quantifies the thermodynamic interaction of PTMA and the solvents of interest. Additionally, a direct fit of the scattering data to the polymer excluded volume model quantifies the expansion of the polymer in solution and complements the Zimm analysis. Comparison of the experimentally determined and theoretically calculated Flory−Huggins interaction parameters emphasizes the importance of accounting for counterions to understand the thermodynamic interactions between the organic radical polymer and solvents. Our analyses also indicate that solvent, radical loading, and temperature all impact the final conformation of PTMA. Finally, an electrochemical study of PTMA as a thin film that is cast from both solvents establishes a correlation between the conformation in solution and the performance of PTMA.

MATERIALS AND METHODS

Materials. The following materials were received from Sigma-Aldrich and used without further purification: toluene (anhydrous, 99.8%), sodium tungstate dihydrate ($Na_2WO_4{\cdot}2H_2O$; 99%), ethylenediaminetetraacetic acid disodium salt dihydrate ($Na_2EDTA{\cdot}2H_2O$; 99.0−101.0%), methanol (99.8%), and magnesium sulfate (anhydrous, 99.5%). 2,2′-Azobis(2-methylpropionitrile) (AIBN; 98%) was received from Sigma-Aldrich and was recrystallized from ethanol before use. The following materials were received from VWR BDH Chemicals and used without any further purification: hexanes (≥98.5%), dichloromethane (DCM; cyclohexene stabilized, ≥99.5%), aqueous hydrogen peroxide solution (30 wt %; sodium stannate stabilized), and methanol (≥99.8%). 2,2,6,6-Tetramethyl-4-piperidyl methacrylate (TMPM; ≥98.0%) was received from TCI America and used without purification. 4-Cyano-4-(((dodecylthio)-carbonothioyl)thio)pentanoic acid (97%) chain transfer agent (CTA) was used as received from Boron Molecular. Ultrapure water (water) was collected from a Milli-Q water purification system (18 MΩ·cm).

Synthesis of PTMA-X-R. The synthetic conditions for the different molar mass PTMA-X-R produced are found in Table 1, where X is the estimated degree of polymerization and R is the radical loading obtained from electron paramagnetic resonance (EPR) spectroscopy. The synthesis of PTMA-276−68 and PTMA-277−98 followed the protocol described by Easley et al.[18] For the remaining PTMA-X-R polymers, the synthetic protocol was modified to use 4-cyano-4-(((dodecylthio)carbonothioyl)thio)pentanoic acid as the CTA (Scheme 1).[18,20]

A summary of the synthetic procedure to synthesize PTMA-15−72 is provided as an example. In a 50 mL Schlenk flask, 5 g (22.2 mmol) of TMPM, 83.9 mg (0.5 mmol) of AIBN, 0.69 g (1.7 mmol) of CTA, and 7.7 mL of toluene were combined at ambient conditions. The

https://doi.org/10.1021/acs.macromol.4c01134
Macromolecules 2024, 57, 6333−6343

flask was sealed, and three freeze−pump−thaw cycles were performed. The flask was left under nitrogen, heated to 75 °C, and left to react for 24 h. The reaction was cooled to room temperature and exposed to air to terminate the reaction. The reaction solution was precipitated in hexanes. The resulting polymer, PTMPM-15-CTA, was collected and dried under vacuum for 24 h. The CTA end groups were removed as previously described, by combining 2 g of PTMPM-15-CTA (8.9 mmol of repeat unit) with 2 g (12 mol) of AIBN in 80 mL of toluene.[18,20] The reaction solution was then heated to 75 °C and left to react for 24 h. After 24 h, the reaction was allowed to reach room temperature before being precipitated in hexanes. The precipitated polymer, PTMPM-15, was collected and vacuum-dried for 24 h. Finally, PTMPM was oxidized using H_2O_2 by reacting 0.6 g of PTMPM-15 (2.6 mmol of repeat unit), 218.8 mg (0.7 mmol) of $Na_2WO_4{\cdot}2H_2O$, 115.8 mg (0.3 mmol) of $Na_2EDTA{\cdot}2H_2O$ in 30 mL of methanol in a 250 mL round-bottom flask equipped with a condenser. The reaction was carried out at 60 °C for 5 min, before 3.0 mL of 30 wt % H_2O_2 was added dropwise. After the addition was complete, the reaction was left at 60 °C for 24 h. The solid precipitate was dissolved in DCM, washed with MQ water three times, and dried over magnesium sulfate for 12 h. The magnesium sulfate was filtered out followed by precipitation of the resulting solution into hexanes. The resulting orange solid (PTMA-15−72) was collected and vacuum-dried overnight.

Chemical Characterization. For NMR, 10 mg of PTMPM-X-CTA or PTMPM-X was dissolved in 1 mL of deuterated chloroform and a 400 MHz Bruker NMR was used to collect the ^{1}H NMR spectra. Size exclusion chromatography (SEC) was performed on a TOSOH EcoSEC (HLC-8320GPC) with UV (254 nm) and RI detectors at 40 °C with THF as the eluent with a flow rate of 0.35 mL min^{-1}. The SEC sample was prepared by dissolving 5 mg of PTMA-X-R in 1.5 mL of THF. The molecular weights were calculated using a calibration curve based on polystyrene standards. The SEC columns were TSKgel SuperHM-M and TSKgel SuperH-RC. Electron paramagnetic resonance (EPR) spectroscopy was performed on a Bruker Elexsys at room temperature. For EPR, a reference solution of 1 mM of 4-OH-TEMPO and a sample solution of 1 mM of polymer repeat unit (PTMA-X) were prepared in chloroform. Using the ultraviolet−visible (UV−vis) calibration curve previously reported by Easley et al., the radical loading of each PTMA-X-R sample solution, prepared at a concentration of 0.03 M (repeat unit basis) in chloroform, was calculated at 462 nm.[18] Finally, XPS spectra were collected on powder samples of the PTMA-X-R samples using an Omicron XPS with an Argus detector using a monochromated Mg X-ray source (hm = 1253.6 eV). Survey scans were performed with an analyzer pass energy of 150−1150 eV (1.0 eV steps, 50 ms dwell time). High-resolution scans of nitrogen (N 1s), chlorine (Cl 2p), and fluorine (F 1s) were collected with a pass energy of 150 eV (0.05 eV steps, 200 ms dwell time). All spectra were calibrated using the C 1s photoemission peak (sp^2-hybridized carbons) at 284.5 eV. Curve fitting of N 1s spectra was conducted using a Gaussian−Lorentzian peak shape after a Shirley-type background correction and the fwhm of the deconvoluted peaks was constrained.

Small-Angle Neutron Scattering (SANS) Experiments. The solvents used for SANS experiments are *N*-methyl-2-pyrrolidinone-d_9 (d-NMP), d_6-dimethyl carbonate (Cambridge Isotope Lab), and d_4-ethylene carbonate (CDN Isotopes, Inc.). SANS experiments of PTMA-276−68 polymer in *N*-methyl-2-pyrrolidinone-d_9 (d-NMP) and a 1:1 (w/w) mixture of d_4-ethylene carbonate and d_6-dimethyl carbonate (d-EC:d-DMC) were performed at the National Institute for Standards and Technology's Center for Neutron Research using the NG-7 beamline with a q range of 0.0042−0.41 Å^{-1}. The SANS experiments of PTMA-15−72, PTMA-44−87, PTMA-122−95, and PTMA-277−98 polymers in *N*-methyl-2-pyrrolidinone-d_9 (d-NMP) were performed at the high flux isotope reactor (HFIR) at the Oak Ridge National Laboratory on the CG-2 GP-SANS beamline with a q range of 0.003−0.7 Å^{-1}. Here, $q = 4\pi/\lambda \sin(\theta)$, where, q is the momentum transfer vector, λ is the neutron wavelength and θ is the scattering angle. The raw data obtained at NIST was reduced using NCNR SANS reduction package,[21] whereas the raw data from HFIR was reduced using the reduction protocol prepared by the instrument scientist. The scattering data of PTMA-X-R was corrected for sample transmission, and the scattering of the empty cell, solvent scattering, and the background. The fitting procedures were performed using SasView software.[22]

Group Contribution and Flory−Huggins Interaction Parameter. The Hansen solubility parameters (HSPs) for PTMA-276−68 and PTMA-277−98 are reported in Table 2 and were estimated using the Hansen group contribution method and values previously published by our group for the nitroxide radical and oxoammonium cation.[18,23] Additionally, the Hansen solubility parameter values for NMP, EC, and DMC were taken from Hansen and are summarized in Table 2 below.[24] It was assumed that the solvent deuteration did not alter the Hansen solubility parameters. Previous studies also showed that small polarizability and vibration energy difference in C-D and C-H result in little to no impact on the solubility parameter of solvents.[25,26]

Table 2. Dispersion (δ_d), Polar (δ_p), Hydrogen Bonding (δ_h), and Total (δ_{total}) Hansen Solubility Parameters for the Polymers and Solvents Utilized

material	δ_d (MPa$^{1/2}$)	δ_p (MPa$^{1/2}$)	δ_h (MPa$^{1/2}$)	δ_{total} (MPa$^{1/2}$)
PTMA-276−68	19.2	4.7	7.5	21.2
PTMA-277−98	19.1	4.7	7.8	21.1
NMP[a]	18.0	12.3	7.2	22.9
EC[a]	19.4	21.7	5.1	29.6
DMC[a]	15.5	3.9	9.7	18.7
EC/DMC (1:1)[b]	17.5	12.8	7.4	24.1

[a]Values from ref 27. [b]Estimated as a 50:50 mixture.

Using the total Hansen solubility parameters, the Flory−Huggins (polymer−solvent) interaction parameter, χ, is determined for each polymer−solvent combination using eq 1.

$$\chi = \frac{V_s}{RT}(\delta_{total,s} - \delta_{total,p})^2 + 0.34 \quad (1)$$

In eq 1, V_s is the molar volume of the solvent (in cm^3/mol), R is the gas constant (8.314 cm^3 MPa/mol K), T is the temperature (in K), and $\delta_{total,s}$ and $\delta_{total,p}$ are the total Hansen solubility parameters for the solvent and polymer, respectively. The molar volumes of NMP, EC, and DMC are 96.5, 66.0, and 84.2 cm^3/mol, respectively. Using these values, the molar volume of the EC/DMC mixture is 75.1 cm^3/mol.

In addition to estimating χ from the total Hansen solubility parameters, it may also be experimentally determined using the second virial coefficient (A_2) from Zimm analysis of the SANS data, following eq 2.[27]

$$\chi = 0.5 - A_2 V_s \rho_p^2 \quad (2)$$

where ρ_p is the density of the polymer (in g/cm^3).

Electrochemical Characterization. PTMA-276−68 and PTMA-277−98 were dissolved in NMP at 2 mg/mL and PTMA-276−68 was also dissolved in EC/DMC (1:1, w/w) at 2 mg/mL. Twenty μL of the polymer solution was drop cast onto a glassy carbon electrode and allowed to dry at ambient conditions for 48 h. After 48 h, the samples were dried under vacuum for an additional 24 h before electrochemical testing. The polymer-coated glassy carbon acted as the working electrode in a three-electrode beaker cell with a Pt wire counter electrode and an Ag/AgCl (sat.) reference electrode. The supporting electrolyte was 0.5 M tetraethylammonium tetrafluoroborate ($TEABF_4$) in water. The polymer thin film was conditioned by cyclic voltammetry (CV) (50 cycles at 50 mV·s^{-1}) before conducting two CV cycles each at varying scan rates (10, 25, 50, and 100 mV·s^{-1}). Chronoamperometry (CA) was performed by a potential step from 0.3 to 1.1 V and retuning to 0.3 V vs Ag/AgCl (all voltages were held for 60 s). Additionally, galvanostatic charge/discharge was performed for 5 cycles at both 20 and 40 μA/cm^2. All

https://doi.org/10.1021/acs.macromol.4c01134
Macromolecules 2024, 57, 6333−6343

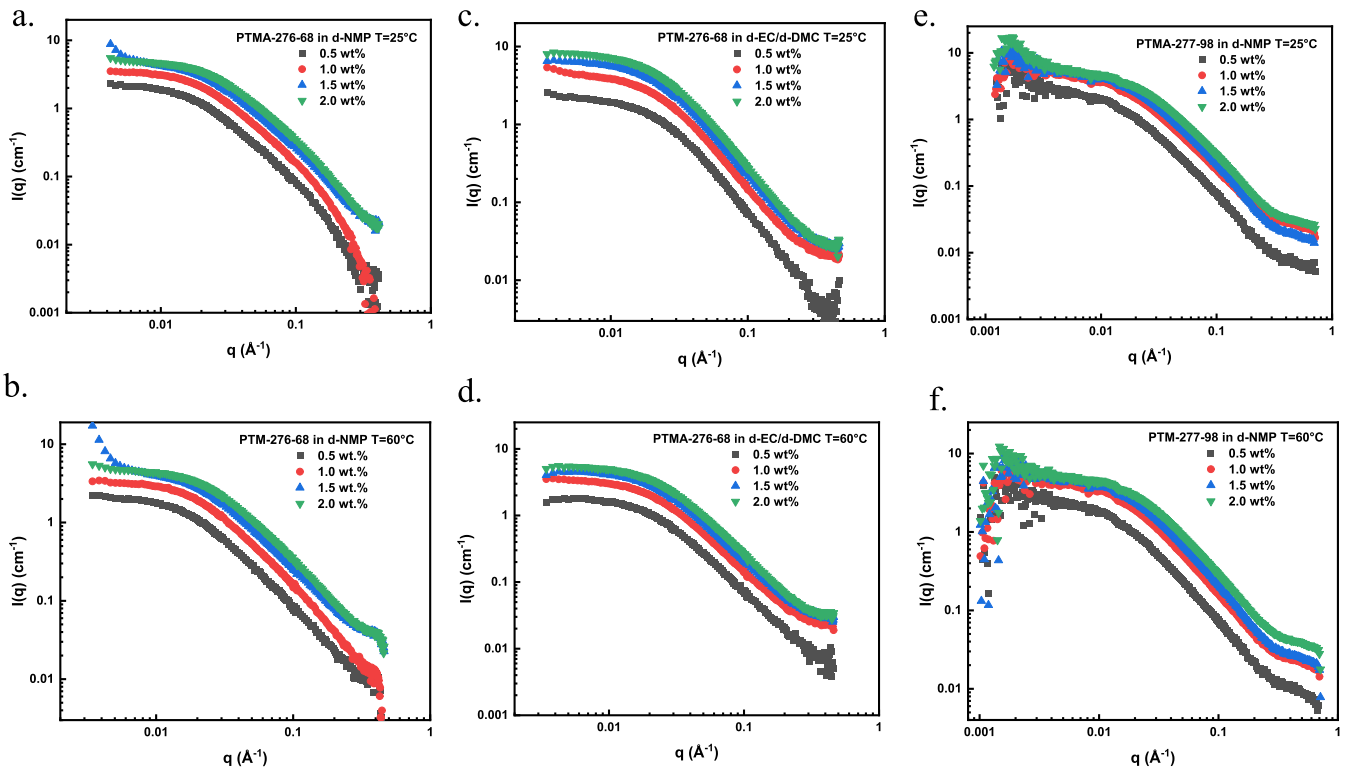

Figure 1. Small-angle neutron scattering profiles of (a) PTMA-276−68 in d-NMP at 25 °C, (b) PTMA-276−68 in d-NMP at 60 °C, (c) PTMA-276−68 in d-EC:d-DMC at 25 °C, (d) PTMA-276−68 in d-EC:d-DMC at 60 °C, (e) PTMA-277−98 in d-NMP at 25 °C, and (f) PTMA-277−98 in d-NMP at 60 °C.

electrochemical measurements were performed using a Solartron Electrochemical Interface 1287 potentiostat/galvanostat.

The CA data was further analyzed to estimate the diffusion coefficient of electron transfer (D_{et}) by fitting using the Cottrell equation (eq 3) assuming semi-infinite condition.[10]

$$i = \frac{nFAC_0^*}{\sqrt{\pi t}}\sqrt{D_{et}} = \tau\frac{nFAC_0^*}{\sqrt{\pi}}\sqrt{D_{et}} \quad (3)$$

where i is the current output from CA (in mA), n is the number of electrons transferred per repeat unit, A is the electrode area (in cm^2), and C_0^* is the total concentration of redox sites (or repeat units in mol/cm^3). Following the method of Paulse et al., the slope was determined from the line tangent to the CA data and the origin (0,0).[28,29] The effective rate constant for electron transfer, k_{eff}, was calculated using the Laviron−Andrieux−Savéant equation (eq 4).

$$k_{eff} = \frac{6D_{et}}{C_0^*\delta^2} \quad (4)$$

From the peak separation of the CV data at 10 mV s^{-1}, the heterogeneous rate constant, k^0, was calculated using the simplified method of Nicholson (eq 5). The simplified form assumed the diffusion coefficient of the oxidized and reduced species is equal to D_{et}.

$$\psi = \frac{k^0}{(\pi D_{et} f\upsilon)^{1/2}} \quad (5)$$

RESULTS

Synthesis and Characterization of PTMA-X-R. The precursor to PTMA-X-R, PTMPM-X, was synthesized using reversible addition−fragmentation chain transfer (RAFT) polymerization, where X is the degree of polymerization and R is the radical loading from electron paramagnetic resonance (EPR) spectroscopy (Scheme 1 and Table 1). The resulting PTMPM-X contained RAFT chain transfer agent (CTA) end groups (PTMPM-X-CTA). The end groups were removed before oxidation to prevent cross-linking.[20] Figures S1−S3 show the ^{1}H NMR spectra for PTMPM-X-CTA and PTMPM-X. The spectra for PTMPM-15- and PTMPM-44- show decreases in the peaks associated with the CTA (between 3 and 3.5 ppm), confirming the successful removal of the CTA end group.

After removing the CTA end group, the PTMPM-X precursors were oxidized with meta-chloroperoxybenzoic acid (mCPBA) or hydrogen peroxide, following previously reported methods to form the PTMA-X-R radical polymers.[20,30,31] The molar mass (and thus degree of polymerization) and dispersity were determined for each polymer using size exclusion chromatography (SEC), where the results are shown in Table 1, and SEC traces are presented in Figure S4. Following oxidation, the radical loading was determined using X-ray photoelectron spectroscopy (XPS) and electron paramagnetic resonance (EPR) spectroscopy. Tables 1 and S1 document the amount of radical loading and pendant group distribution in each PTMA-X-R sample. The XPS and EPR spectra are also documented in Figures S5 and S6. XPS was critical for determining the distribution of functional groups, amine, nitroxide radical, and oxoammonium cation groups, for each PTMA-X-R sample. The different groups result from no oxidation, oxidation, and overoxidation of the polymer, respectively. Utilizing the above PTMA-X-R samples, various analyses were considered to determine the structural characteristics of PTMA-X-R in d-NMP and d-EC:d-DMC using SANS. The structural parameters are determined from analyses of the scattering patterns, including Guinier[32,33] and Zimm anal-

https://doi.org/10.1021/acs.macromol.4c01134
Macromolecules 2024, 57, 6333−6343

yses[33,34] to describe the size and conformation of the polymer and Zimm analysis to gain insights on the thermodynamic interaction parameter between the solvent and the polymer. The molecular weight dependence of the radius of gyration for the synthesized PTMA-X-R is determined to elucidate the effect of radical content on the polymer conformation. Finally, analysis of the polymer conformation by fitting to the polymer excluded volume model[35−38] quantitively reveals the compactness of the PTMA-X-R chain, highlighting the variation of the polymer chain conformation in different solvents at 25 and 60 °C.

Guinier and Zimm Analysis of PTMA-X-R in Solution. SANS scattering profiles of PTMA-276−68 in d-NMP and d-EC:d-DMC and PTMA-277−98 in d-NMP at room temperature and 60 °C are shown in Figure 1. To determine the radius of gyration of the PTMA-X-R polymer in individual solvents, the Guinier model, documented as eq 6, is used.[32,33]

$$\ln[I(q)] = \ln[I(0)] - \frac{q^2 \times {R_g}^2}{3} \tag{6}$$

Here, R_g is the radius of gyration, q is the wave vector and $I(0)$ is the forward scattering intensity. The Guinier model emerges from expanding the relationship between the measured scattering intensity and the Fourier transform of the density distribution function of a single particle to a power series, which is only valid at low q, giving $I(q) = I(0)\exp(-1/3\, q^2 {R_g}^2)$. Equation 6 is the linearized version of this relationship. In these equations, $I(0)$ is the forward scattering intensity at $q = 0$, and corresponds to the total number of scattering particles (i.e., polymer chains) in the scattered volume. The total number of scattering particles (polymer chains) can be determined from the scattering particle (polymer) concentration, polymer molecular weight, and specific volume, where this relationship leads to eq 7, which correlates the $I(q = 0)$ to the molecular weight of the PTMA-X-R polymer.[39]

$$I(0) = \frac{M_w \times d \times N_A}{\varphi \times \Delta\rho^2} \tag{7}$$

In eq 7, M_w is the weight average molecular weight of PTMA-X-R polymer, d is the density of the PTMA-X-R polymer, N_A is Avogadro's number, φ is the volume fraction of the PTMA-X-R polymer in solution and $\Delta\rho$ is the difference in scattering cross-section of the polymer and solvent. The radius of gyrations and molecular weights of all the PTMA-X-R studied as obtained from the Guinier analysis are listed in Table 3.

The intraparticle interference of scattering from different segments of the same chain impacts the measured scattering intensity. This results in an angular dependence of the scattering, as shown in eq 8.[33,34]

Table 3. Molecular Weight (M_w) and Radius of Gyration (R_g) from Guinier Analysis of the Scattering of 1 wt % PTMA-X-R in Respective Solvents

sample name	solvent (temperature)	M_w (kg/mol)	$R_g \pm$ error (Å)
PTMA-276−68	d-NMP (25 °C)	155	65 ± 2
PTMA-276−68	d-NMP (60 °C)	146	66 ± 2
PTMA-276−68	d-EC:d-DMC (25 °C)	142	71 ± 4
PTMA-276−68	d-EC:d-DMC (60 °C)	142	69 ± 3
PTMA-277−98	d-NMP (25 °C)	130	100 ± 5
PTMA-277−98	d-NMP (60 °C)	130	96 ± 3

$$\frac{K\varphi}{I(q)} = \frac{1}{M_w}\left(1 + \frac{q^2 {R_g}^2}{3}\right) + 2A_2\varphi \tag{8}$$

In eq 8, $K = \Delta\rho^2 V_m \varphi / N_A$ is the contrast factor, V_m is the molar volume of PTMA-X-R (202.5 cm^3/mol), φ is the volume fraction of PTMA-X-R in solution, N_A is the Avogadro's constant, M_w is the PTMA weight average molecular weight, A_2 is the second virial coefficient which describes the polymer−solvent interactions. A common method to analyze small-angle scattering data is the Zimm plot that employs a double extrapolation of the data to both zero concentration and zero scattering angle where Zimm analysis provides information on the quality of the solvent, as well as serves as a supplement to the Guinier analysis by providing the M_w and R_g of the polymer. An example Zimm plot is provided in Figure S7.

However, our initial Zimm analysis, the results of which are tabulated in Table S2, shows a significant variation in the molecular weight of PTMA-X-R in different solvent conditions. This is physically unreasonable and must be an artifact of the analysis. To identify this artifact, the concentration dependence of the scattering of PTMA-X-R in each solvent was investigated. Scattering theory shows that the q dependence of the scattering intensity of a sample ($I(q)$) is directly proportional to the contrast between the scattering particle and its surroundings ($\Delta\rho^2$), the concentration of scattering particles (c), the form factor that accounts for intraparticle correlations of a scattering particle ($F(q)$) and the structure factor that accounts for interparticle correlations between scattering particles ($S(q)$), as shown in eq 9.[33,39]

$$I(q) \sim \Delta\rho^2 \times c \times F(q) \times S(q) \tag{9}$$

For our experiments, $\Delta\rho^2$ is the difference in the scattering length density of the solvent and the polymer. The scattering length density (SLD) of each atomic species can be calculated from its density and atomic composition. Initially, the SLD of PTMA-X-R, and the solvents d-NMP and d-EC:d-DMC are calculated to be 0.918×10^{-6}, 6.20×10^{-6}, and 5.40×10^{-6} $Å^{-2}$, respectively. $F(q)$ in eq 9 is the form factor that depends on the structure/conformation of the PTMA polymer. Lastly, $S(q)$ is the structure factor that details the particle-to-particle interaction, where, in our samples, since the polymer solution is dilute, the $S(q)$ is 1.

Therefore, if the coherent scattering of PTMA-X-R in a given solvent is normalized by the concentration of the polymer, eq 9 shows that the scattering profiles should overlap. When normalized to concentration, the PTMA-276−68 dissolved in d-EC:d-DMC at 25 °C shows the expected collapse of all scattering curves, as shown in Figure 2. In contrast, the normalization of the scattering curves with concentration of all other solutions showed a decrease in scattering intensity with an increase in concentration, as shown in Figure 3, with additional examples provided in Figure S8.

Equation 9 shows that the most likely parameter that could account for this unexpected result is an incorrect value of the scattering length density of the solvent, which translates to an incorrect value of $\Delta\rho^2$ in eq 9. We interpret this to indicate that the molecular composition of the solvent is not pure NMP or EC/DMC, but must include the presence of counterions associated with the PTMA.[18] These counterions alter the SLD of the solvent and must be accounted for. Moreover, this also emphasizes that the scattering length densities of the solvent for a series of concentrations are not constant; rather, it varies

https://doi.org/10.1021/acs.macromol.4c01134
Macromolecules 2024, 57, 6333−6343

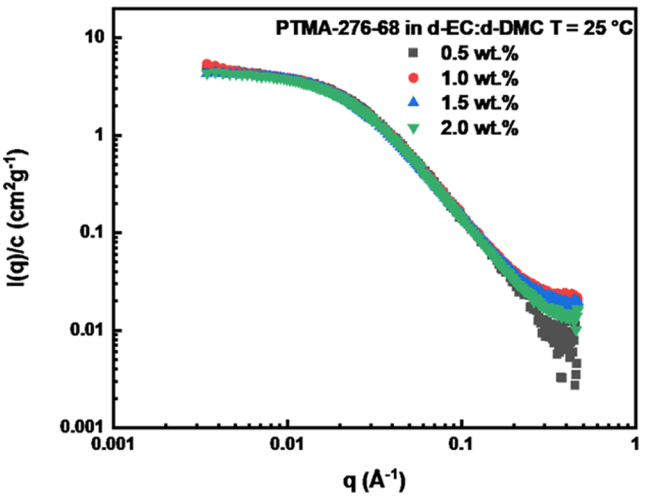

Figure 2. Normalized SANS scattering profile of PTMA-276−68 in d-EC:d-DMC provides a master curve.

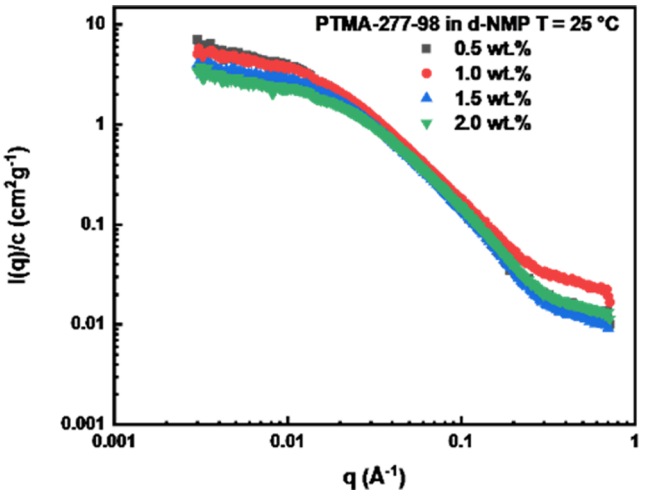

Figure 3. Normalized SANS scattering profiles of PTMA-277−98 in d-NMP emphasizing the absence of scaling with concentration.

with the amount of counterion in the solvent. The results show that the SLD of the solvent decreases with increasing PTMA (and counterion). To account for this deviation of the solvent SLD from the SLD of the pure solvent, the corrected SLD, which accounts for counterion present, is determined from eq 10.

$$\Delta\rho^2_{\text{corrected}} = \frac{\Delta\rho^2_{\text{theoretical}} \times I(0)_{\text{experiment}}}{I(0)_{\text{theoretical}}} \quad (10)$$

In eq 10, $\Delta\rho_{\text{corrected}}{}^2$ is the corrected contrast between solvent and polymer to account for the presence of the counterion whereas $\Delta\rho_{\text{theoretical}}{}^2$ is the theoretical contrast between the pure solvent and polymer, $I(0)_{\text{experimental}}$ is the forward scattering of the experimental SANS profile of PTMA-X-R polymer and $I(0)_{\text{theoretical}}$ is the forward scattering of the SANS profile obtained using eq 6, where M_w= molecular weight of the PTMA-X-R polymer obtained from Guinier analysis= ~142 kg/mol, d = density of the polymer, N_A= Avogadro's number, φ= volume fraction of the polymer. The fact that the scattering of the room temperature solution of PTMA-276−68 in d-EC:d-DMC scales with concentration enables the use of the molecular weight value obtained from the Guinier analysis of this sample in these calculations. Following this approach provides the proper contrast parameter $\Delta\rho^2$ of all the polymer solutions, resulting in scattering patterns that scale with concentration, and can be analyzed by the Zimm analysis.

Figure S9 plots the SLD of the solvent as a function of PTMA concentration for the d-EC:d-DMC solutions at 60 °C, where extrapolation of the SLD to zero PTMA concentration gives a value of the SLD (5.20×10^{-6} Å^{-2}) that is very similar to that of the estimated SLD of the pure d-EC:d-DMC mixture (5.40×10^{-6} Å^{-2}). Therefore, the SLD of the solvent is corrected to account for counterions, and the data is then reanalyzed. For example, Figure 4 shows the scattering curves

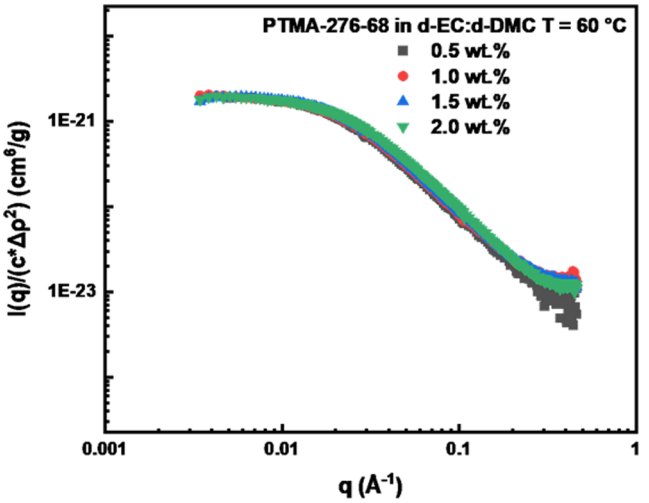

Figure 4. Corrected scattering profile of PTMA-276−68 in d-EC:d-DMC at 60 °C.

of the PTMA-276−68 in d-EC:d-DMC at 60 °C normalized to concentration, where the data collapse to a single curve. The results of the Zimm analyses of the SLD corrected data for all solutions are presented in Table 4.

Inspection of the Zimm analysis results presented in Table 4 shows consistent molecular weights of the PTMA for all solutions. The modest variation in molecular weight of PTMA-277−68 in d-NMP with temperature is attributed to the low signal-to-noise ratio of the scattering profile. Although the second virial coefficient shows variation with the change in solvents and temperature, these values are at least an order of magnitude smaller than A_2 of a polymer in a good solvent (10^{-4}−10^{-5} mol cm^3 g^{-2}) and are therefore close to 0. This indicates that all the solvents are marginal solvents for the PTMA polymer under all conditions. However, the subtle variation in second virial coefficients resonates with the variation of the radius of gyration of the PTMA polymer in d-NMP and d-EC:d-DMC. For instance, the radius of gyration of PTMA-276−68 is 90 Å in d-NMP at 25 °C, whereas in d-EC:d-DMC the radius of gyration decreases to 80 Å, which corresponds to a slight decrease in the A_2 and the quality of the solvent.

Similarly, the A_2 of PTMA-277−98 in d-NMP is marginally higher than that of the PTMA-276−68 in d-NMP, suggesting that NMP is a slightly better solvent (though still marginal) for the polymer with higher radical content. It is interesting that although the A_2 of the PTMA-277−98 in d-NMP is modestly greater than that of PTMA-276−68 in d-NMP, the radius of gyration of the PTMA-277−98 increases by *ca.* 27 Å. We

https://doi.org/10.1021/acs.macromol.4c01134
Macromolecules 2024, 57, 6333−6343

Table 4. Summary of Second Virial Coefficients (A_2), Radius of Gyration (R_g), and Molecular Weights (M_w) of PTMA-276-68 in d-NMP and d-EC:d-DMC and PTMA-277-98 in d-NMP at 25 and 60 °C

sample name	solvent, temperature	$A_2 \pm$ error (mol cm^3 g^{-2})	M_w (kg/mol)	$R_g \pm$ error (Å)
PTMA-276−68	d-NMP, T = 25 °C	$3.09 \times 10^{-6} \pm 2.015 \times 10^{-6}$	141	90 ± 5
PTMA-276−68	d-NMP, T = 60 °C	$7.69 \times 10^{-6} \pm 9.05 \times 10^{-7}$	143	85 ± 4
PTMA-276−68	d-EC:d-DMC, T = 25 °C	$-2.37 \times 10^{-6} \pm 3.60 \times 10^{-6}$	144	80 ± 4
PTMA-276−68	d-EC:d-DMC, T = 60 °C	$9.64 \times 10^{-7} \pm 3.93 \times 10^{-7}$	142	75 ± 4
PTMA-277−98	d-NMP, T = 25 °C	$6.20 \times 10^{-6} \pm 4.71 \times 10^{-6}$	143	117 ± 6
PTMA-277−98	d-NMP, T = 60 °C	$1.56 \times 10^{-5} \pm 1.41 \times 10^{-5}$	150	111 ± 6

interpret this to indicate that the repulsion between radicals on the same chain dominates the conformation more than the polymer−solvent interaction, where the increase in radical content from 68 to 98% forces the PTMA chain to expand in the d-NMP. This repulsion is an important consideration in the electron transfer rate within a solvent-swollen polymer electrode.

Polymer Excluded Volume Analysis. The scattering of a polymer chain that obeys a Gaussian polymer chain, which models a polymer chain in the melt, was first derived by Debye, which shows that the scattering intensity decays with a power law of −2 at high q.[40] This power law, d, is inversely proportional to the Flory exponent, ν, that correlates the radius of gyration of a polymer chain to its molecular weight, $R_g \sim M_w^{\nu}$−$d = 1/\nu$. However, the same polymer chain in a good solvent will expand due to excluded volume, decreasing the power law dependence of the scattering. This expansion of the polymer chain in a good solvent is captured by the polymer excluded volume model.[35−38]

Thus, the SANS curves of the samples were fit to the polymer excluded volume model, which provides the radius of gyration and Flory exponent ν for each sample. As a reminder, a Flory exponent, ν = 0.5, indicates that the polymer chain attains a random walk conformation, which corresponds to the conformation of a coiled polymer in a theta solvent. A Flory exponent, 0.5 < ν < 0.60, corresponds to an expanded polymer chain, where the transition of ν from 0.5 to 0.6 indicates an improvement in solvent quality and a self-avoiding walk has ν = 0.6. A polymer chain with ν > 0.6 corresponds to a semiflexible polymer chain.[41]

Figure S10 shows a representative fit of the scattering of the 0.5 wt % PTMA-276−68 in d-NMP sample at 60 °C to the polymer excluded volume model. Table 5 summarizes the Flory exponents and radii of gyration of all 0.5 wt % solutions of PTMA-X-R at different temperatures.

The data in Table 5 shows that the variation in the radius of gyration of the polymer corresponds well to the Flory exponent, where a larger Flory exponent leads to an increase in the size of the polymer chain. Moreover, an increase in temperature, which usually corresponds to improved solvent quality, leads to further increases in both the Flory exponent and polymer radius of gyration for all three samples. The data also are consistent with the observation that NMP is a better solvent for the PTMA than EC/DMC, as for both temperatures PTMA-276−68 attains a larger R_g and Flory exponent, indicating a more expanded conformation. This analysis is consistent with the Zimm analysis that showed that the R_g of this polymer in d-EC:d-DMC is about 10 Å smaller than in d-NMP. The data also provides insight into the impact of radical loading on the polymer conformation. The R_g and Flory exponent of the PTMA with higher radical loading, PTMA-277−98, in d-NMP are larger than those of PTMA-276−68, which has a similar molecular weight. We interpret this to indicate that the higher radical loading results in intrachain repulsions that manifest as an increase in polymer chain expansion.

Table 5. Polymer Excluded Volume Parameters of 0.5 wt % PTMA-X-R Solutions at 25 and 60 °C

sample mame	radius of gyration T = 25 °C	Flory exponent T = 25 °C	radius of gyration T = 60 °C	Flory exponent T = 60 °C
PTMA-276−68 in d-NMP	79 Å ± 1	0.52	83 Å ± 1	0.55
PTMA-276−68 in d-EC:d-DMC	68 Å ± 1	0.45	73 Å ± 1	0.50
PTMA-277−98 in d-NMP	98 Å ± 2	0.56	102 Å ± 1	0.58

It is interesting that the radii of gyration reported in the polymer excluded volume analysis are generally smaller than those reported by the Zimm analysis. We ascribe this variation to the complexity of the Zimm analysis, which requires fitting the scattering intensity that emerges from extrapolating to zero concentration. The multistep process introduces more uncertainty in the reported R_g values that are reported in Table 4, which may be the source of this variation.

Polymer−Solvent Interaction Parameters for PTMA Solutions. To compare the conformation determined using SANS to other indicators of solvent quality, the Flory−Huggins (polymer−solvent) interaction parameter, χ, was determined from the experimentally determined second virial coefficient. χ larger than 0.5 indicates a "poor" solvent, whereas values smaller than 0.5 indicate a "good" solvent, and χ values of 0.5 typically indicate a theta solvent. In a good solvent, an expanded chain is expected due to favorable interactions between the polymer and solvent. In contrast, in a poor solvent, a collapsed chain is expected to minimize interactions between the polymer and solvent. Using the total Hansen solubility parameters for the polymers and solvents, χ was calculated for both polymers in d-NMP and PTMA-276−68 in d-EC:d-DMC using eq 1 (summarized as group contributions in Table 6). Additionally, the A_2 values from Zimm analysis were used to calculate the experimentally determined interaction parameters from eq 2.

As expected, as the temperature increases from 25 to 60 °C, the calculated χ value decreases, indicating more favorable interactions between the polymer and solvent, which should correlate to a more expanded chain conformation. Overall, χ values obtained from group contribution analysis indicate that NMP is a good solvent for the polymer (χ < 0.5) and EC/DMC is a poor solvent (χ > 0.5) for the polymer. However, the experimentally determined χ values do not show this same solvent and temperature dependence. All of the SANS-determined χ values indicate a marginal solvent that is very

https://doi.org/10.1021/acs.macromol.4c01134
Macromolecules 2024, 57, 6333−6343

Table 6. Polymer−Solvent Interaction Parameters (χ) Calculated from the Second Virial Coefficient (SANS) and from Group Contribution Estimates of the Polymer Solubility Parameters (Group Contribution)

		group contribution		SANS	
polymer	solvent	$\chi_{25\ °C}$	$\chi_{60\ °C}$	$\chi_{25\ °C}$	$\chi_{60\ °C}$
PTMA-276−68	d-NMP	0.38	0.37	0.50	0.50
	d-EC:d-DMC	0.64	0.60	0.50	0.50
PTMA-277−98	d-NMP	0.36	0.35	0.50	0.50

close to a theta solvent, regardless of temperature or solvent. These results strongly suggest that the approximations that are used in calculating the χ values using group contribution analysis overestimate the similarity of the Hansen Solubility parameters of the polymer and solvent. Given the importance of the presence of counterions in the analyses of the scattering curves, we suspect that not accounting for the presence of the counterion in estimating the polymer−solvent thermodynamic interactions is a significant source of error. Therefore, future attempts to estimate χ values of radical polymers must account for the presence of the counterion in group contribution analysis.

It is interesting that the Flory exponents in Table 5 indicate a change in solvent quality from a theta solvent (ν = 0.5) to a good solvent (ν = 0.58), but this is not observed in the reported χ parameters. We ascribe this to the fact that the χ parameter is a mean field global parameter, while subtle changes in polymer conformation are dependent on local intermolecular interactions and thus the two may not always respond proportionally. For instance, the presence of the counterion may alter the local dielectric constant, which may change and impact polymer conformation but not the global χ parameter.

Molecular Weight Dependence of R_g. The dependence of the radius of gyration of a polymer chain with molecular weight provides central information about its conformation. With that in mind, Figure 5 plots the molecular weight dependence of the radius of gyration of PTMA chains that were oxidized using H_2O_2 in d-NMP. The oxidation with H_2O_2 results in polymers with higher oxidation than those oxidized with mCPBA. This analysis of the variation of R_g with chain length therefore provides further insight into the impact of the increased radical loading that emerges from the H_2O_2 oxidation on the conformation of the PTMA chain. The R_g of the PTMA chains oxidized by H_2O_2 in 1 wt % solution as determined from the Guinier model fit of the scattering profiles is plotted as a function of the $I(q = 0)$, which is proportional to the polymer molecular weight in Figure 5. The data are fit to a power law in Figure 5, which shows that the dependence of $R_g \propto I(0)^{0.63}$. This slightly larger Flory exponent is greater than that of a polymer chain that follows self-avoiding walk statistics.[41] The observed exponent of 0.63 further quantifies the extent to which the PTMA polymer with higher radical content can be thought of semiflexible, as it is slightly more rigid than a Gaussian coil.

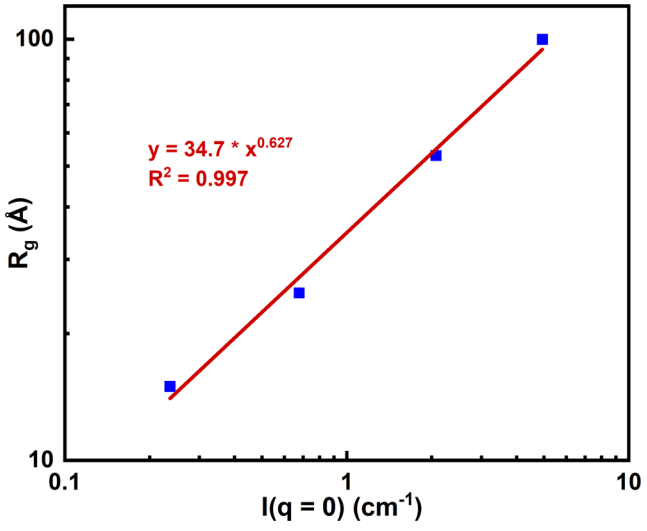

Figure 5. Log R_g vs log I(0) plot of PTMA-X-R oxidized by H_2O_2 with similar high oxidation levels in d-NMP at 25 °C.

Electrochemistry of PTMA. The electrochemical properties of PTMA thin films of different oxidation levels cast from different solvents were investigated using cyclic voltammetry (Figure 6) and galvanostatic charge/discharge in a three-electrode beaker cell with PTMA thin film on a glassy carbon working electrode, Pt wire counter electrode, Ag/AgCl (sat.) reference electrode, and 0.5 M $TEABF_4$ in water as supporting electrolyte. The cyclic voltammograms demonstrate that regardless of oxidation method and casting solvent PTMA-X-R exhibited similar half-wave ($E_{1/2}$) redox potentials of 0.78 V vs Ag/AgCl at 10 mV/s. Similarly, all of the films exhibited a linear relationship between peak current and the square root of scan rate, which is indicative of a diffusion-limited reaction.

In contrast, there were distinct differences in the slope of the linear relationship between peak current and the square root of scan rate for the three samples. In oxidation, the PTMA-276−68 thin film cast from EC/DMC had the largest slope, followed by PTMA-276−68 cast from NMP, and PTMA-277−98 cast from NMP. These slope values, from Figure S12, were used to determine the apparent diffusion coefficient of electron transfer (D_{et}) following the Randles-Sevcik equation (eq 11).

$$i_p = (2.69 \times 10^5) n^{3/2} A C D_{et}^{1/2} v^{1/2} \quad (11)$$

where I_p is the peak current (A), n is the number of electrons, A is the electrode area (cm^2), C is the concentration of redox-active sites (mol/mL), v is the scan rate (V/s), and D_{et} is the apparent diffusion coefficient of electron transfer (cm^2/s). This analysis results in D_{et} of 3.0×10^{-13} cm^2/s for the PTMA-276−68 EC/DMC cast film and 1.5×10^{-14} cm^2/s for both the PTMA-276−68 and PTMA-277−98 NMP cast films. As shown in Table 7, the kinetic rate constants obtained from chronoamperometry (Figure S13) show a similar trend with casting solvent.

The more compact structure of PTMA-276−68 in EC/DMC suggests that the films contain globular compact coils, which might lead to denser cast films relative to NMP. The denser film could, in turn, facilitate intra- and interchain electron transfer, leading to higher rate constants and apparent electron diffusivities This interpretation hinges on the correlation of predeposition solution state conformations to their assembly in the solvent-swollen polymer thin films, where experimental studies offer evidence of this correlation.[42−45] The improved kinetics manifested in a significantly larger discharge capacity for PTMA cast from EC/DMC as compared to casting from NMP (450 vs 100 mAh cm^{-2}, respectively) in Figure S14.

https://doi.org/10.1021/acs.macromol.4c01134
Macromolecules 2024, 57, 6333−6343

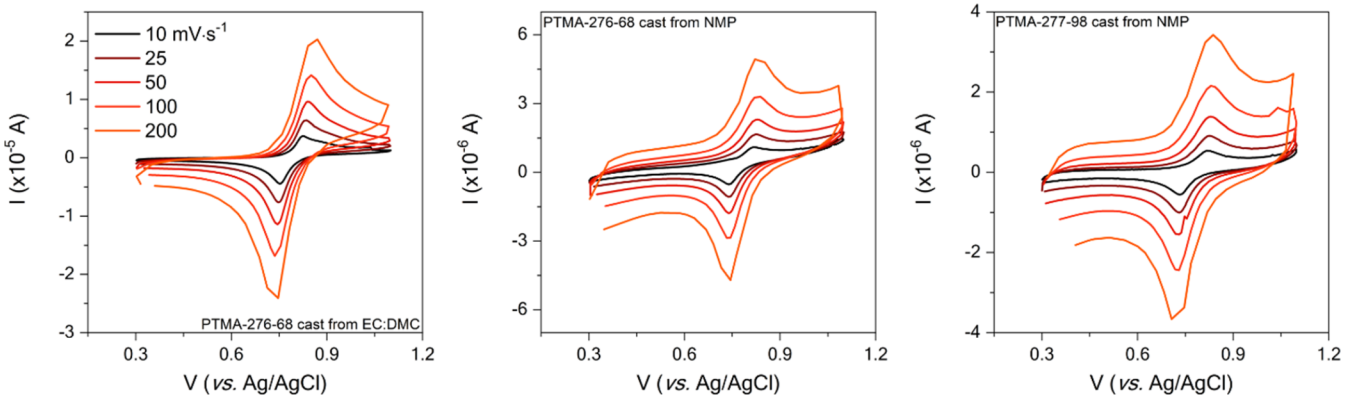

Figure 6. Cyclic voltammograms for PTMA-276−68 thin films cast from (left) EC/DMC solution and (center) NMP solution and for (right) PTMA-277−98 cast from NMP solution. The cyclic voltammograms were obtained in a three-electrode beaker cell with the PTMA-X-R thin films on glassy carbon working electrodes, Pt wire counter electrode, Ag/AgCl (sat.) reference electrode, and 0.5 M $TEABF_4$ as supporting electrolyte in water.

Table 7. Electron Transfer Rate Constants for PTMA-X-R Thin Films Cast from Two Different Solvents

polymer	casting solvent	log (k_{eff}) [log(L/mol·s)]	log (D_{et}) [log(cm^2/s)]	log (k^0) [log(cm/s)]
PTMA-276−68	EC/DMC	2.6	−12.4	−6.1
	NMP	1.0	−14.0	−7.0
PTMA-277−98		0.8	−14.2	−7.3

DISCUSSION

Previous studies have clearly shown that the conformation of a polymer in a predeposition solvent dramatically impacts the morphology and assembly of functional polymer films, which directly impacts its performance.[42−45] This leads us to the conclusion that to understand the charge transport of nonconjugated PTMA polymer, it is imperative to understand the conformation of the polymer in solvents that are frequently used in the fabrication and operation of batteries. Moreover, previous theoretical and experimental studies have shown that the PTMA polymer conformation and assembly vary with radical loading.[15,46] Therefore, to rationally guide the design and fabrication of organic radical polymers, a more thorough understanding of the impact of polymer molecular weight, radical loading, and temperature in battery-relevant solvents is needed. Small-angle neutron scattering experiments provide the structure, assembly, and thermodynamic interactions of PTMA-X-R chains in battery-relevant solvents. Interestingly, the initial Zimm analysis clearly indicates that the solvent is more complex than initially thought. Careful consideration revealed that the counterions that are present in the solution must be accounted for in further analyses of the scattering data. With this correction, the Zimm analysis provides second virial coefficients that quantify the polymer−solvent thermodynamic interactions, which indicates that all the solvents are marginal for the PTMA chains regardless of solvent, temperature, molecular weight, or radical loading. Moreover, comparison of the estimated Flory−Huggins interaction parameter from Hansen parameter group contributions and the SANS-derived experimental values shows significant discrepancies. These inconsistencies are attributed to the assumption that the counterion does not impact the polymer−solvent interaction in the calculated estimation of χ.

The Zimm analysis also provides the radius of gyration of the polymers as a function of solvent, temperature, and radical loading, which are consistent with the polymer excluded volume analysis. These analyses demonstrate that the PTMA polymer chains expands in d-NMP more than it does in the d-EC:d-DMC, where the radius of gyration of the PTMA with more radical loading, PTMA-277−98, is significantly larger than that of the PTMA with lower radical loading, PTMA-276−68. This indicates that the molecular conformation of the organic radical polymer is dominated by the amount of radical loading present in the polymer backbone more than the solvent type and temperature. These results clearly indicate that increasing the radical loading increases the stiffness in the backbone of PTMA-X-R polymer. The increase in rigidity in the polymer backbone with increased radical loading has also been observed by Martin et al. in deuterated acetonitrile.[15]

This information on the conformation and thermodynamic interactions of PTMA-X-R polymer in different solvents correlates with the electrochemical performance of the polymer in solid state formed from these solvents. The higher apparent diffusion coefficient in the PTMA-276−68 film cast from EC/DMC is consistent with the compact shape of the polymer in solution, which forces the TEMPO radicals to assemble close to each other, allowing for more rapid charge transfer in the system. Previous theoretical studies have also provided evidence of increased charge diffusion in PTMA films when the PTMA chains are more collapsed to ease the hopping of the electron from one radical to another.[46] This work suggests that use of a processing solvent that results in a collapsed chain conformation when casting electrodes will help to enhance the rate of charge transfer and improve the capacity performance.

CONCLUSIONS

Small-angle neutron scattering results document the conformation, assembly, and thermodynamic interactions of PTMA-X-R in battery-relevant solvents. These results document the impact of solvent, radical loading, and temperature on polymer conformation. Careful Zimm analysis demonstrates that the presence of counterions in the solvent must be accounted for in the analyses. When these are accounted for, it is clear that the NMP and EC/DMC are marginal solvents for the PTMA. Moreover, comparison of these experimental χ values to those found from Hansen parameter group

https://doi.org/10.1021/acs.macromol.4c01134
Macromolecules 2024, 57, 6333−6343

calculations emphasizes the need to account for the presence of the counterion in determining the polymer−solvent interaction parameter, χ using Hansen parameter group calculations.

Further correlation of the SANS-determined second virial coefficients to the R_g indicates the NMP is a marginally good solvent and EC/DMC is a marginally poor solvent for the PTMA chains. This corresponds to a slightly swollen PTMA chain in d-NMP and a slightly collapsed PTMA chain in d-EC:d-DMC. The polymer excluded volume analysis further quantifies the change in the PTMA conformation with a change in solvent or radical loading. These results show that the PTMA chain with lower radical loading, PTMA-276−68 attains a self-avoiding walk conformation while the PTMA chain with the higher radical loading, PTMA-277−98, expands and attains a more semirigid conformation. Similarly, for both radical loadings polymer excluded volume dimension analysis shows that an increase in temperature contributes to further expansion of the polymer chain. A holistic interpretation of the entire analyses presented emphasizes that the conformation of the organic radical PTMA chain is primarily driven by the radical loading, while solvent choice and temperature are important, but secondary governing factors.

Moreover, the electrochemical performance of PTMA films formed from each solvent is consistent with these conformations. The electrochemical results suggest that the radicals of PTMA-276−68 in EC/DMC are more closely packed, as would be expected with a more compact conformation, which drives improved inter and intrachain charge diffusion. Finally, future efforts should focus on the identification of electrode processing solvents that result in a collapsed chain conformation of the organic radical polymer leading to improved capacity performance in organic batteries.

■ ASSOCIATED CONTENT

Supporting Information

The Supporting Information is available free of charge at https://pubs.acs.org/doi/10.1021/acs.macromol.4c01134.

NMR curves, SEC traces, XPS data and analysis, and EPR data of synthesized PTMA; example Zimm Plot and results of Zimm Plot analysis; example scattering profiles and fits to models; and results of electrochemical analysis of the synthesized PTMA (PDF)

■ AUTHOR INFORMATION

Corresponding Author

Mark D. Dadmun − *Department of Chemistry, University of Tennessee, Knoxville, Tennessee 37996, United States;* orcid.org/0000-0003-4304-6087; Email: Dad@utk.edu.

Authors

Md Ashraful Haque − *Department of Chemistry, University of Tennessee, Knoxville, Tennessee 37996, United States*

Alexandra D. Easley − *Department of Material Science & Engineering, Texas A&M University, College Station, Texas 77840, United States*

Josh G. Moncada − *Department of Chemistry, University of Tennessee, Knoxville, Tennessee 37996, United States*

Jodie L. Lutkenhaus − *Department of Material Science & Engineering, Texas A&M University, College Station, Texas 77840, United States; Department of Chemical Engineering, Texas A&M University, College Station, Texas 77840, United States;* orcid.org/0000-0002-2613-6016

Complete contact information is available at: https://pubs.acs.org/10.1021/acs.macromol.4c01134

Notes

The authors declare no competing financial interest.

■ ACKNOWLEDGMENTS

Research supported as part of the Breakthrough Electrolytes for Energy Storage (BEES), an Energy Frontier Research Center funded by the U.S. Department of Energy (DOE), Office of Science, Basic Energy Sciences (BES), under Award DE-SC0019409 (neutron scattering experiments and analysis). We acknowledge the support of the National Institute of Standards and Technology, U.S. Department of Commerce, in providing the neutron research facilities used in this work. A portion of this research was also completed at the High Flux Isotope Reactor a DOE Office of Science User Facility operated by the Oak Ridge National Laboratory. This work benefited from the use of the SasView application, originally developed under NSF award DMR-0520547. SasView contains code developed with funding from the European Union's Horizon 2020 research and innovation program under the SINE2020 project, grant agreement No 654000. An acknowledgment is made to the Donors of the American Chemical Society Petroleum Research Fund for partial support of this work (solubility parameter). This work was supported by grant DE-SC0014006 funded by the US Department of Energy, Office of Science (electrochemistry). A.D.E. acknowledges support by the National Science Foundation Graduate Research Fellowship under Grant No. DGE:1746932.

■ REFERENCES

(1) Helms, B. A.; Seferos, D. S. Virtual Issue: Designing Polymers for Use in Electrochemical Energy Storage Devices. *Macromolecules* **2019**, *52*, 1349−1353, DOI: 10.1021/acs.macromol.9b00035.

(2) Kim, J. K.; Cheruvally, G.; Choi, J. W.; Ahn, J. H.; Lee, S. H.; Choi, D. S.; Song, C. E. Effect of Radical Polymer Cathode Thickness on the Electrochemical Performance of Organic Radical Battery. *Solid State Ionics* **2007**, *178* (27−28), 1546−1551.

(3) Li, M.; Lu, J. Cobalt in Lithium-Ion Batteries. *Science* **2020**, *367* (6481), 979−980.

(4) Li, W.; Lee, S.; Manthiram, A. High-Nickel NMA: A Cobalt-Free Alternative to NMC and NCA Cathodes for Lithium-Ion Batteries. *Adv. Mater.* **2020**, *32* (33), No. 2002718.

(5) Kang, D. H. P.; Chen, M.; Ogunseitan, O. A. Potential Environmental and Human Health Impacts of Rechargeable Lithium Batteries in Electronic Waste. *Environ. Sci. Technol.* **2013**, *47* (10), 5495−5503.

(6) Wei, X.; Xu, W.; Vijayakumar, M.; Cosimbescu, L.; Liu, T.; Sprenkle, V.; Wang, W. TEMPO-Based Catholyte for High-Energy Density Nonaqueous Redox Flow Batteries. *Adv. Mater.* **2014**, *26* (45), 7649−7653.

(7) Nishide, H.; Iwasa, S.; Pu, Y. J.; Suga, T.; Nakahara, K.; Satoh, M. Organic Radical Battery: Nitroxide Polymers as a Cathode-Active Material. *Electrochim. Acta* **2004**, *50* (2−3), 827−831.

(8) Yonekuta, Y.; Susuki, K.; Oyaizu, K.; Honda, K.; Nishide, H. Battery-Inspired, Nonvolatile, and Rewritable Memory Architecture: A Radical Polymer-Based Organic Device. *J. Am. Chem. Soc.* **2007**, *129* (46), 14128−14129.

(9) Tan, Y.; Casetti, N. C.; Boudouris, B. W.; Savoie, B. M. Molecular Design Features for Charge Transport in Nonconjugated Radical Polymers. *J. Am. Chem. Soc.* **2021**, *143* (31), 11994−12002.

(10) Wang, S.; Easley, A. D.; Lutkenhaus, J. L. 100th Anniversary of Macromolecular Science Viewpoint: Fundamentals for the Future of Macromolecular Nitroxide Radicals. *ACS Macro Lett.* **2020**, *9* (3), 358−370.
(11) Nakahara, K.; Oyaizu, K.; Nishide, H. Organic Radical Battery Approaching Practical Use. *Chem. Lett.* **2011**, *40*, 222−227, DOI: 10.1246/cl.2011.222.
(12) Loo, W. S.; Mongcopa, K. I.; Gribble, D. A.; Faraone, A. A.; Balsara, N. P. Investigating the Effect of Added Salt on the Chain Dimensions of Poly(Ethylene Oxide) through Small-Angle Neutron Scattering. *Macromolecules* **2019**, *52* (22), 8724−8732.
(13) McCulloch, B.; Ho, V.; Hoarfrost, M.; Stanley, C.; Do, C.; Heller, W. T.; Segalman, R. A. Polymer Chain Shape of Poly(3-Alkylthiophenes) in Solution Using Small-Angle Neutron Scattering. *Macromolecules* **2013**, *46* (5), 1899−1907.
(14) Annis, B. K.; Kim, M. H.; Wignall, G. D.; Borodin, O.; Smith, G. D. Study of the Influence of LiI on the Chain Conformations of Poly(Ethylene Oxide) in the Melt by Small-Angle Neutron Scattering and Molecular Dynamics Simulations. *Macromolecules* **2000**, *33* (20), 7544−7548.
(15) Martin, H. J.; Hughes, B. K.; Braunecker, W. A.; Gennett, T.; Dadmun, M. D. The Impact of Radical Loading and Oxidation on the Conformation of Organic Radical Polymers by Small Angle Neutron Scattering. *J. Mater. Chem. A* **2018**, *6* (32), 15659−15667.
(16) Bugnon, L.; Morton, C. J. H.; Novak, P.; Vetter, J.; Nesvadba, P. Synthesis of Poly(4-Methacryloyloxy-TEMPO) via Group-Transfer Polymerization and Its Evaluation in Organic Radical Battery. *Chem. Mater.* **2007**, *19* (11), 2910−2914.
(17) Basma, N. S.; Headen, T. F.; Shaffer, M. S. P.; Skipper, N. T.; Howard, C. A. Local Structure and Polar Order in Liquid N-Methyl-2-Pyrrolidone (NMP). *J. Phys. Chem. B* **2018**, *122* (38), 8963−8971.
(18) Easley, A. D.; Vukin, L. M.; Flouda, P.; Howard, D. L.; Pena, J. L.; Lutkenhaus, J. L. Nitroxide Radical Polymer−Solvent Interactions and Solubility Parameter Determination. *Macromolecules* **2020**, *53*, 7997−8008, DOI: 10.1021/acs.macromol.0c01739.
(19) Bauer, W.; Nötzel, D. Rheological Properties and Stability of NMP Based Cathode Slurries for Lithium Ion Batteries. *Ceram. Int.* **2014**, *40* (3), 4591−4598.
(20) Rostro, L.; Baradwaj, A. G.; Boudouris, B. W. Controlled Radical Polymerization and Quantification of Solid State Electrical Conductivities of Macromolecules Bearing Pendant Stable Radical Groups. *ACS Appl. Mater. Interfaces* **2013**, *5* (20), 9896−9901.
(21) SANS and USANS Data Reduction and Analysis Software | NIST. https://www.nist.gov/ncnr/data-reduction-analysis/sans-software. (accessed May 12, 2024).
(22) SasView - Small Angle Scattering Analysis. https://www.sasview.org/. (accessed May 12, 2024).
(23) Hansen, C. *The Three Dimensional Solubility Parameter and Solvent Diffusion Coefficient and Their Importance in Surface Coating Formulation*; Danish Technical Press: Copenhagen, 1967.
(24) Barton, A. F. M.*CRC Handbook of Solubility Parameters and Other Cohesion Parameters*, 2nd ed.; Routledge, 2017; pp 1−739.
(25) Budkowski, A.; Rysz, J.; Scheffold, F.; Klein, J.; Fetters, L. J. Effect of Deuterium Substitution on the Surface Interactions in Binary Polymer Mixtures. *J. Polym. Sci., Part B: Polym. Phys.* **1998**, *36* (15), 2691−2702.
(26) Lee, B.; Littrell, K.; Sha, Y.; Shevchenko, E. V. Revealing the Effects of the Non-Solvent on the Ligand Shell of Nanoparticles and Their Crystallization. *J. Am. Chem. Soc.* **2019**, *141* (42), 16651−16662.
(27) Orofino, T. A.; Flory, P. J. Relationship of the Second Virial Coefficient to Polymer Chain Dimensions and Interaction Parameters. *J. Chem. Phys.* **1957**, *26* (5), 1067−1076, DOI: 10.1063/1.1743472.
(28) Paulse, C. D.; Pickup, P. G. Chronoamperometry of Polypyrrole: Migration of Counterions and Effect of Uncompensated Solution Resistance. *J. Phys. Chem. A* **1988**, *92* (24), 7002−7006.
(29) Ma, T.; Li, C. H.; Thakur, R. M.; Tabor, D. P.; Lutkenhaus, J. L. The Role of the Electrolyte in Non-Conjugated Radical Polymers for Metal-Free Aqueous Energy Storage Electrodes. *Nat. Mater.* **2023**, *22* (4), 495−502.
(30) Wang, S.; Li, F.; Easley, A. D.; Lutkenhaus, J. L. Real-Time Insight into the Doping Mechanism of Redox-Active Organic Radical Polymers. *Nat. Mater.* **2019**, *18* (1), 69−75.
(31) Zhang, Y.; Park, A.; Cintora, A.; McMillan, S. R.; Harmon, N. J.; Moehle, A.; Flatté, M. E.; Fuchs, G. D.; Ober, C. K. Impact of the Synthesis Method on the Solid-State Charge Transport of Radical Polymers. *J. Mater. Chem. C* **2018**, *6* (1), 111−118.
(32) Guinier, A.; Fournet, G. *Small-Angle Scattering of X-Rays*; John Wiley & Sons, Inc: New York, 1955.
(33) Roe, R.-J. *Methods of X-ray and Neutron Scattering in Polymer Science*; Oxford University Pres: Oxford, 2000.
(34) Zimm, B. H. The Scattering of Light and the Radial Distribution Function of High Polymer Solutions. *J. Chem. Phys.* **1948**, *16* (12), 1093−1099.
(35) Benoit, H. The diffusion of light by polymers dissolved in a good solvent. *Comptes Rendus* **1957**, *245*, 2244−2247.
(36) Hammouda, B. SANS from Homogeneous Polymer Mixtures - A Unified Overview. *Adv. Polym. Sci.* **1993**, *106*, 87−133.
(37) Hore, M. J. A.; Hammouda, B.; Li, Y.; Cheng, H. M. Co-Nonsolvency of Poly(N-isopropylacrylamide) in Deuterated Water/Ethanol Mixtures. *Macromolecules* **2013**, *46*, 7894−7901.
(38) Hammouda, B.; Kim, M.-H. The empirical core-chain model. *J. Mol. Liq.* **2017**, *247*, 434−440.
(39) Higgins, J. S.; Benoit, H. C. *Polymers and Neutron Scattering*; Oxford University Pres: Oxford, 1994.
(40) Debye, P. Molecular-weight Determination by Light Scattering. *J. Phys. Colloid Chem.* **1947**, *51* (1), 18−32.
(41) Hiemenz, P. C.; Lodge, T. P. *Polymer Chemistry*; Taylor & Francis: New York, 2007.
(42) Heroux, L.; Moncada, J.; Dadmun, M. D. Controlling the Morphology of PEDOT:PSS Blend Films with Pre-Deposition Solution Composition and Deposition Technique. *ACS Appl. Polym. Mater.* **2022**, *4* (1), 36−43.
(43) Etampawala, T.; Tehrani, M.; Nematollahi, A.; He, L. L.; Dadmun, M. The impact of solvent doping on the morphology and performance of spray-coated PEDOT:dPSS: A USANS and SANS study. *Org. Electron.* **2017**, *51*, 86−93.
(44) Murphy, R. J.; Weigandt, K. M.; Uhrig, D.; Alsayed, A.; Badre, C.; Hough, L.; Muthukumar, M. Scattering Studies on Poly(3,4-ethylenedioxythiophene)-Polystyrenesulfonate in the Presence of Ionic Liquids. *Macromolecules* **2015**, *48* (24), 8989−8997.
(45) Zabihi, F.; Xie, Y.; Gao, S.; Eslamian, M. Morphology, conductivity, and wetting characteristics of PEDOT:PSS thin films deposited by spin and spray coating. *Appl. Surf. Sci.* **2015**, *338*, 163−177.
(46) Kemper, T. W.; Larsen, R. E.; Gennett, T. Relationship between Molecular Structure and Electron Transfer in a Polymeric Nitroxyl-Radical Energy Storage Material. *J. Phys. Chem. C* **2014**, *118* (31), 17213−17220.

https://doi.org/10.1021/acs.macromol.4c01134
Macromolecules 2024, 57, 6333−6343